

Article

Investigation of Electrodeposition External Conditions on Morphology and Texture of Ni/SiC_w Composite Coatings

Liyang Lai, Hongfang Li , Yunna Sun, Guifu Ding * , Hong Wang and Zhuoqing Yang

National Key Laboratory of Science and Technology on Micro/Nano Fabrication, School of Electronic Information and Electrical Engineering, Shanghai Jiao Tong University, Shanghai 200240, China

* Correspondence: gfding@sjtu.edu.cn; Tel.: +86-21-34206686

Received: 19 August 2019; Accepted: 9 September 2019; Published: 12 September 2019



Abstract: Recently, a strategy of synthesizing SiC whisker-reinforced nickel (Ni/SiC_w) composites with excellent mechanical properties by electrodeposition has been proposed for exploring its potential applications in micromechanical devices. In this paper, a series of external conditions that affected the content of SiC whiskers in composite films were studied, such as cathode current density, stirring rate and electrolyte temperature. The experimental results indicated that the optimum morphology was obtained at a stirring speed of 300 rpm, a temperature of 50 °C, and a current density of 18 mA/cm². Additionally, the content of SiC whiskers and textural preference were also investigated by varying its external conditions, and the results demonstrated that the composites with high mass percentage whiskers are more advantageous for electrocrystallization of Ni in the (200) orientation. Finally, the relationship between external conditions and intrinsic morphology, composition and texture of Ni/SiC_w composites was revealed, and it provides a constructive approach to fabricate the high-content SiC whiskers of these composites.

Keywords: physical conditions; electrodeposition; SiC whisker; texture; morphology

1. Introduction

Electrodeposition is one of the most commercially successful and inexpensive superior techniques for fabrication of metallic coatings. However, the conventional electrodeposition methods are very simple, since it has only one phase throughout the process. The pure electroplated metals are difficult to satisfy the current requirements, due to their plastic deformation. In order to resolve this problem, the method of co-deposition insoluble solid particles in metal matrix was established and recognized for fabrication the composite coatings. The reinforcing particles, suspending in the electrolyte, are entrapped and incorporated into the metal matrix by adopting suitable methods during the co-deposition process, such as electrophoresis, adsorption or mechanical entrapment [1]. In 1928, Fink et al. [2] introduced the co-deposition method to produce Cu/graphite composite coatings that applied in car engines for the first time. Besides, the first patent of co-deposition was issued by Grazen, in 1962 [3]. Since then, considerable researches have been focused on different types of composites fabricated by the co-deposition method. These composites include ceramics, metals, polymer or microcapsule/liquid incorporated into metal matrices, which could improve the coating properties as mechanical strength, wear/friction-resistance, high-temperature oxidation-resistant and corrosion-resistance [4–15]. Based on the SiC_w with features in high modulus and tensile strength, good wear resistance, as well as dimensional stability, recently, we have successfully synthesized high mechanical strength Ni/SiC_w composites by electrodeposition.

Since the performance of composite coatings is highly sensitive to external conditions during the co-deposition process, such as current density, temperature, stirring speed, and current density, etc.

Therefore, numerous efforts have been dedicated to improving its microstructure and micromorphology of the deposited coatings for enhancing their properties. Lately, relevant studies have revealed that the content of particles in the composite coating can be controlled by the external conditions during the deposition process, and resulting in a difference in the performance of the composite coatings. H. Gül et al. [16] reported the nickel metal matrix composites reinforced with SiC submicron particles by electrodeposition. Besides, the influence of stirring speed and particles concentration on co-deposited composite coatings was investigated. The results indicated that the maximum of particle concentration was 20 g/L and the high stirring speed was chosen to obtain the wear resistant nickel matrix coatings. P. Gyftou et al. [17] applied both direct and pulse current conditions to produce Ni/ nano-SiC composites, and it proved that pulse electrodeposition significantly improved the hardness of the Ni/SiC composite deposits. C.K. Chung et al. [18] investigated the electrodeposition process of Ni at low electrolytic temperatures (5–20 °C). It demonstrated that low temperature could enhance the hardness up to 6.18 GPa and produce the smoothness of films. Tushar Borkar et al. [19] presented the effects of the deposition conditions and the nanoparticle concentration in the electrolyte on the surface microstructure, crystallographic micro-texture, microhardness, and tribological properties of coatings. The reinforcement of Ni-Al₂O₃ nanoparticles significantly improved microhardness and wear resistance of the composite coatings. Based on the previous studies, it is necessary to clearly understand the influence of various conditions on the co-deposition of SiC whiskers in the nickel matrix, so as to consciously control the whiskers content and effectively manipulate the performance of the composite coatings. The purpose of this study is to achieve high SiC whiskers content in Ni/SiCw composite coatings. In addition, the influence of the parameters, such as stirring speed, electrolyte temperature and cathode current density on the SiCw content in composites were investigated, which clearly indicated the relationship between the external conditions and the content of SiC whiskers in the composites.

2. Materials and Preparation

The SiC whiskers (β - SiCw, XFNANO Material Co., Ltd., Nanjing, China), with an average length of 50 μm and diameter of 0.2 μm , were selected. Ni/SiCw composite coatings were prepared by a constant-current electrodeposition method from a nickel sulfamate electrolyte containing SiC whiskers as a reinforcement phase. Prior to the SiCw addition into the electroplating solution, it was first stirred in 3 vol. % hydrofluoric acid and refluxed for 8 h at 95 °C [20], then ultrasonically washed in distilled water until the pH becomes neutral, subsequently modified by γ -aminopropyltriethoxysilane (KH550). These treatments can remove the SiCw surface impurities (SiO₂) and improve its wettability, as well as dispersibility. After the above treatments, SiC whiskers were added in the electrolyte by continuous magnetically stirring with a rate of 300 rpm for at least 24 h, which can prevent whiskers agglomeration and maintain them in suspension state. According to a number of optimization experiments, the optimal whisker concentration in the electrolyte was 0.8 g/L. The electrolyte composition and electrodeposition parameters are listed in Table 1. Analytical reagents and deionized water were used to prepare the plating solution. After electrodeposition, Ni/SiCw composite coatings were ultrasonically cleaned in distilled water for 10 min to remove loosely adsorbed SiCw from the surface.

The surface morphology and microstructure of the composite coatings were characterized by scanning electron microscopy (SEM; ULTRA55, Zeiss, Germany). The amount of embedded SiCw was evaluated by the energy dispersive X-ray spectroscopy (EDS) with the same system of SEM. The phase structure analysis of the coatings was conducted by X-Ray Diffraction (XRD, D8 Advance, Bruker-axs) operating with Cu K α ($\lambda = 1.54178 \text{ \AA}$) radiation at room temperature. The preferred XRD orientation index $TC(hkl)$ was calculated, and the texture co-efficient (TC) for each (hkl) reflection is given by [21,22]:

$$TC(hkl) = \frac{I_{(hkl)}/I_{0(hkl)}}{\frac{1}{n} \sum I_{(hkl)}/I_{0(hkl)}} \quad (1)$$

where $TC(hkl)$ is the texture coefficient of the specific (hkl) plane; $I(hkl)$ and $I_0(hkl)$ are the diffraction intensity of the electrodeposited nickel and the powder pattern in the JCPDS cards, respectively; n is the number of reflection peaks used in the calculation. Three peaks of (111), (200) and (221) are used to calculate the texture coefficient.

Table 1. Operating parameters for Ni/SiCw composite electroplating.

Electrolyte Composition		Electrodeposition Parameters	
Ni(NH ₂ SO ₃) ₂ ·4H ₂ O	300 g/L	Current density	2~40 mA/cm ²
NiCl ₂ ·6H ₂ O	40 g/L	Temperature	20~60 °C
H ₃ BO ₃	30 g/L	Magnetic stirring	0~500 rpm
SiC whisker	0.8 g/L	pH	4.1

3. Results and Discussions

3.1. Effects of Electrodeposition Parameters on Morphology and Composition of the Ni/SiCw Composite

Figure 1 shows the surface morphology of various current density for the Ni/SiCw composite coatings, which was prepared at a stirring speed of 300 rpm, a temperature of 50 °C, and a current density from 2 mA/cm² to 40 mA/cm². As shown in Figure 1, obviously, the microstructure and content of SiCw in coatings were appreciably affected by the current density. When the current density was lower than 18 mA/cm², the glossy surface of the nickel matrix with uniformly distributed SiC whiskers could be seen, and the content of SiCw increased with the increase of current density (Figure 1a–d). However, when the current density was higher than 25 mA/cm², the whiskers content reduced, and the surface morphology of coatings became nodular and inhomogeneous (Figure 1e–f). These phenomena made clear that the electrodeposits prepared at low current density tend to form smooth and luminous surface morphology with fine grains.

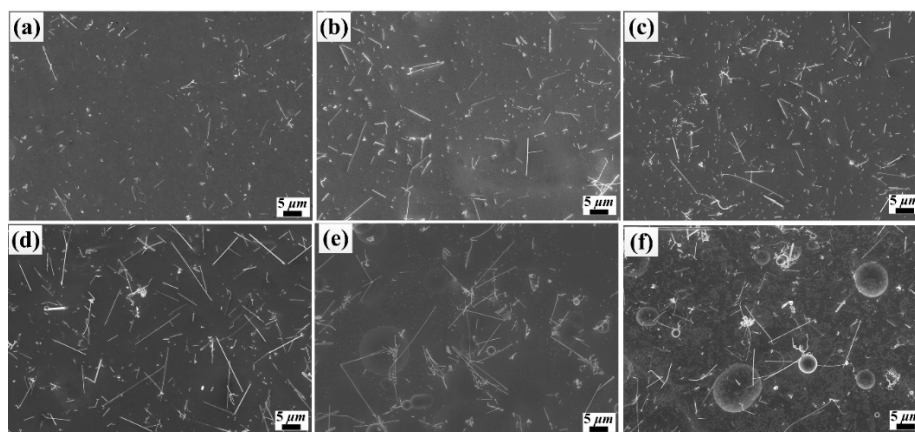


Figure 1. SEM images of Ni/SiCw composite coating fabricated from the electrolyte at stirring speed of 200 rpm, and temperatures of 35 °C, and current density of (a) 2 mA/cm², (b) 6 mA/cm², (c) 10 mA/cm², (d) 18 mA/cm², (e) 25 mA/cm², (f) 40 mA/cm².

The influences of current density on composite coatings could be explained by the following aspects. Firstly, as the cathode current density increases, the Coulomb force between the whisker-adsorbed metal ions and the cathode increases, which can increase the deposition rate of the matrix metal and save time for SiCw to be embedded in Ni matrix. That is, the content of SiCw in the nickel matrix increases at per unit time. Secondly, as the cathode current density increases, the cathode overpotential and the electric field force increases correspondingly, which facilitates the electrostatic attraction of the cathode to the solid particles adsorbing the positive ions. At higher overvoltage, the transportation of metal ions to cathode becomes an important factor in electrodeposition, and it is well known that

the addition of inert particles could enhance this transportation [23]. Compared with lower current density, the rate of whisker that transfer to cathode surface and embed into the composite coatings increases remarkably when the cathode current density is too high. Thirdly, part of the surface of the cathode is covered by whiskers, due to its embedding behavior, which results in the increase of the cathode overpotential, the enhancement of hydrogen adsorption capacity and the formation of alkaline salts near the cathode [4]. These by-products that adsorbed on the cathode surface or embedded into the coating also prevent the whisker from co-depositing with nickel metal and lead to a decrease of the SiCw content in electrodeposits. Besides, at a higher overpotential, the dendrites or nodules were formed on the coating's surface, due to the discharge of metal ions near the cathode, which cause the discharge at the swelling of deposits and it is consistent with previous literature reported by other researchers [2].

During the electrodeposition process, the deposited crystal and grew behavior are closely related to the electrolyte temperature, which plays an essential role in controlling its texture and grain size. Moreover, the mass transfer process of metal ions and whiskers to the cathode surface could be enhanced at an appropriate electrodeposition temperature [24]. Therefore, it is indispensable to evaluate the effect of electrolyte temperature on the composite for the purpose of obtaining the high content of SiCw in the coating with smooth and uniform morphology. In this experiment, the temperature of electrolyte ranging from 20 °C to 60 °C were investigated at a stirring speed of 200 rpm and a current density 18 mA/cm². As illustrated in Figure 2, the dendrites and nodules could be observed clearly at a lower temperature (Figure 2a), while the smooth and luminous surface accompanied by the increasing whisker content was obtained at a temperature rising to 50 °C (Figure 2d). In addition, the nickel grains became finer, and the composite coatings were also strengthened after adding the whiskers. However, the whiskers tended to aggregate and decreased its content in composite coatings when the temperature was exceeding 50 °C, which resulted in the deposited grains was coarse and oversized.

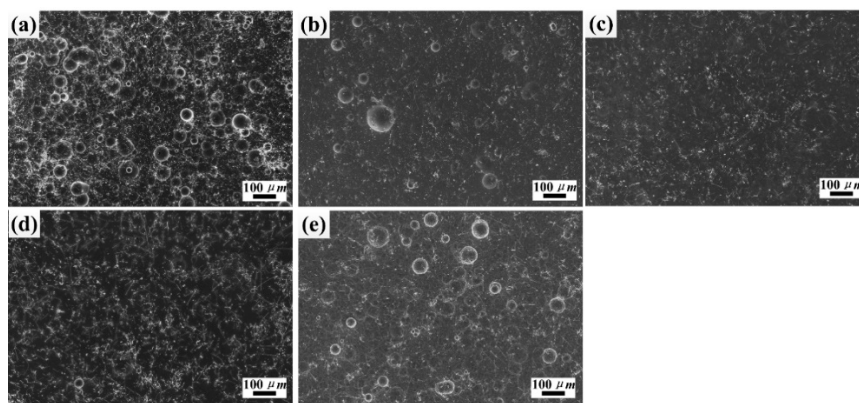


Figure 2. SEM images of Ni/SiCw composite coating fabricated from the electrolyte at stirring speed of 200 rpm, and current density of 18 mA/cm², and temperatures of (a) 20 °C, (b) 30 °C, (c) 40 °C, (d) 50 °C, (e) 60 °C.

In general, both the average kinetic energy of ions and the viscosity of electrolytic could be consolidated by increasing the electrolyte temperature, which all consequently facilitates the transportation of whiskers. Besides, the diffusion mobility of metal ions adsorbed on the cathode surface would be increased on the electrode surface, which resulted in an increase of the whiskers contents in composites coating. Whereas, the anions diffusion rate, the overpotential and the electric field force of the cathode reduced when the temperature reached to a specific value, which was detrimental to the whiskers embedded into the nickel matrix. In addition, the electrolyte would evaporate seriously at a higher temperature, thus, affecting the deposition of active ingredients onto the cathode and coursing the surface of composites. As a result, the excessively high temperature led

to a reduction of the SiCw adsorption ability and the cathode electric field force, which ultimately reduced the SiCw content in the composite coatings.

In order to prevent the precipitation and agglomeration of SiCw in the electrolyte, mechanical stirring was adopted as a key technology in electroplating process, due to the high surface energy of the SiCw. Particularly, the content of particles in composite coatings is depended largely on the strength of stirring, which is advantageous to the uniform distribution of particles in electrolyte and the successful transportation to cathode surface [23]. Figure 3 shows the SEM images relating to the morphology of Ni/SiCw coatings fabricated at a different stirring speed. The conditions of current density and temperature were 18 mA/cm^2 and $50 \text{ }^\circ\text{C}$, and the stirring speed was controlled at 0, 100, 300, and 500 rpm, respectively. Due to the gravity, a large number of whiskers accumulated and covered the major cathode surface without stirring, which resulted in an increase of the cathode overpotential and a decrease of the discharged metal ions near the cathode. Therefore, metal ions discharged at the corner and appeared dendrites or nodules in the composite coatings under the condition without stirring. With the increasing strength of stirring, the mass transfer rate of electrolyte and the effective concentration of whisker were also increased accordingly, which could promote the transportation of SiCw and increase the whisker content in the composite coatings. However, the electrolyte flew at a high speed when the stirring strength is higher than 300 rpm, which caused intense shock to the cathode surface, led to high-speed transfer of the electrolyte accompanied by whiskers and suppressed the attachment of whiskers to the cathode surface. More seriously, whiskers that were not fully embedded in the nickel matrix might be released from the cathode surface to the electrolyte, which resulted in a dramatic decrease of the whisker content in the composite coatings.

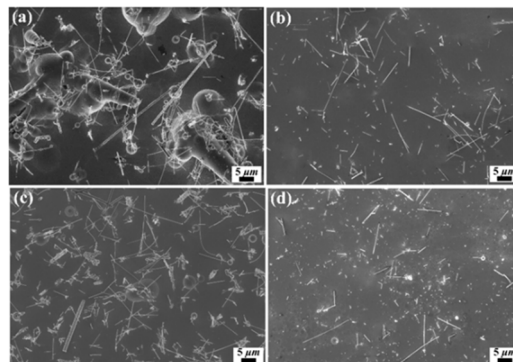


Figure 3. SEM images of Ni/SiCw composite coating fabricated from the electrolyte at a current density of 18 mA/cm^2 , and temperatures of $50 \text{ }^\circ\text{C}$, and stirring speed of (a) 0 rpm, (b) 100 rpm, (c) 300 rpm, (d) 500 rpm.

The cross-sectional SEM images of Ni/SiCw composite coatings prepared with different electrodeposited conditions were shown in Figure 4. From Figure 4a,b, in which the current density ranges from 2 to 8 mA cm^{-2} , an increase in the number of SiCw (pointed by an arrow), which are fairly well dispersed in the nickel matrix, can be clearly observed on the fracture surface. According to the micrographs of the cross section, the fracture surface does not represent the initial interface between the the nickel matrix and SiCw after breaking with external force, so the interface was further illustrated after treatment by an ion beam thinner (Figure 4c,d). From the cross-sectional images of the thinned surface, the whiskers were cut in an identical plane, but in different orientations, due to their random distribution in the the nickel matrix; meanwhile, multiple shapes of whiskers after thinning by ion beam thinner were also noticed.

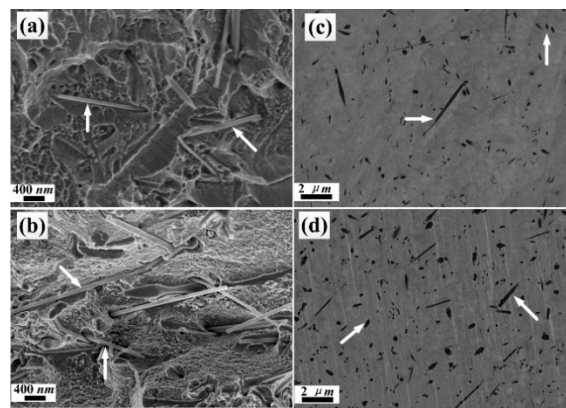


Figure 4. SEM images of the cross section for the fracture (a,b) and thinned surface (c,d) of the electrodeposited Ni/SiCw composite coatings (a) SiCw 0.8 g L⁻¹, 2 mA/cm², 35 °C, 150 rpm; (b) SiCw 0.8 g L⁻¹, 18 mA/cm², 35 °C, 150 rpm; (c) and (d) represent the thinned surface of (a) and (b), respectively.

The EDS spectra of Ni/SiCw composite coatings, prepared at different conditions, are illustrated in Figure 5; and is related to the EDS spectra, which has been listed, as shown in Table 2. As shown in Figure 5a, only Ni peaks were observed in the sample without SiCw coating, whereas the peaks of Ni, Si and C were all collected in Figure 5b–e. The EDS results indicated that the SiC whiskers were incorporated into the nickel matrix successfully. Besides, the obviously increased content of Si and C could be seen from Figure 5b,c, which was resulted from the increased current density from 2 to 18 mA/cm². Since the co-deposition rate of SiCw was strongly related to that of Ni matrix in the process of electrodeposition, then increasing current density could promote the deposition rate of matrix metals and save the time of SiCw embedding into the Ni matrix. In Figure 5c,d, the EDS spectra of the Ni/SiCw coatings deposited at 35 °C and 50 °C, which showed that the higher temperature facilitated the increase of whiskers content in electrodeposits. It shows that the higher temperature facilitates the increase of whiskers content in electrodeposits. As to the influence of stirring speed on the content of SiCw, the stronger stirring speed can contribute to the whiskers transmitting to the cathode surface from the electrolyte which results in its higher content in coatings (Figure 5e).

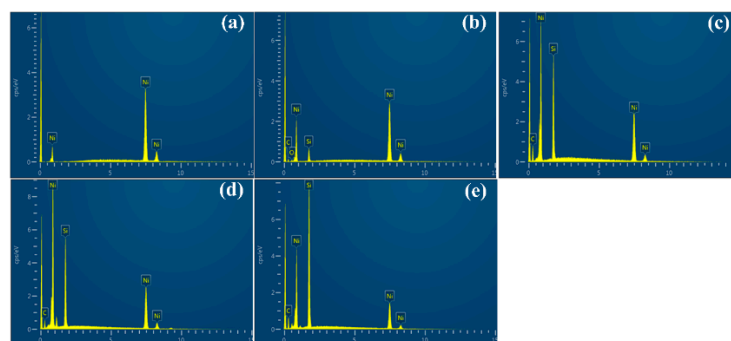


Figure 5. EDS spectra of electrodeposited Ni/SiCw composite coatings (a) without SiCw, 2 mA/cm², 35 °C, 150 rpm; (b) SiCw 0.8 g L⁻¹, 2 mA/cm², 35 °C, 150 rpm; (c) SiCw 0.8 g L⁻¹, 18 mA/cm², 35 °C, 150 rpm; (d) SiCw 0.8 g L⁻¹, 18 mA/cm², 50 °C, 150 rpm; (e) SiCw 0.8 g L⁻¹, 18 mA/cm², 50 °C, 300 rpm.

Table 2. Weight fraction of the composite coatings as deposited at different conditions.

Samples	Weight Fraction (wt. %)			
	Ni	Si	C	O
a	98.66	—	0.32	1.02
b	95.18	1.47	0.55	2.80
c	90.88	3.48	1.00	4.64
d	85.57	5.39	1.48	5.56
e	76.32	8.83	4.67	10.18

3.2. Effects of Electrodeposition Parameters on Crystallographic Texture of the Ni/SiCw Composite Coatings

For all the electrodeposited coatings, the nickel crystals are face-centered cubic structures (FCC). The three peaks at $2\theta = 44.5$, 51.85 and 76.37° that corresponds to (111), (200) and (220) crystallographic planes of nickel respectively, are in agreement with the standard XRD pattern JCPDS 04-0850. Note that the peaks corresponding to the SiCw were not detected in the XRD pattern of the composites. This might be due to the high content of Ni and its high scattering factor leading to higher peak intensities compared to those of SiCw [25]. Figure 6 shows the XRD pattern for the applied SiC whiskers. Comparing to the standard card, SiC particles was fit to No. 29-1129 exactly.

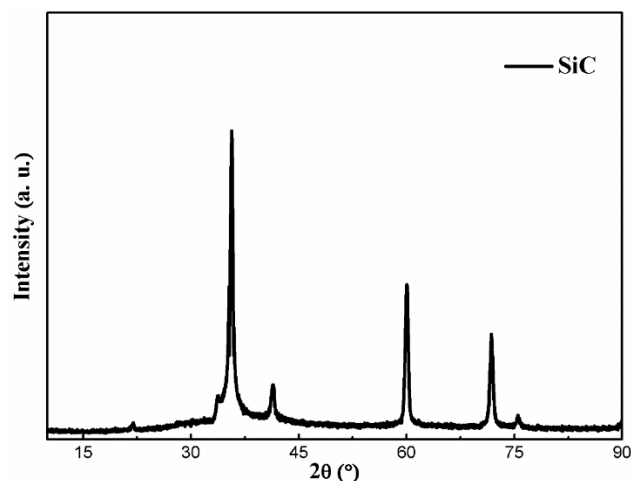
**Figure 6.** XRD pattern of the SiC whiskers.

Figure 7 shows the XRD patterns and its crystallographic orientation indexes of the Ni/SiCw composite coatings fabricated at a different current density. As shown in Figure 7a, at low current density ($2 \text{ mA}\cdot\text{cm}^{-2}$), the composite coating exhibits a strong (111) plane preferred orientation and a relatively low intensity of peaks (200) and (220). However, the intensity of (111) and (220) peak gradually reduce with the increase of current density, while the (200) peak increased obviously. Particularly, when the current density increased to $40 \text{ mA}\cdot\text{cm}^{-2}$, the value of (200) peak intensity reaches the strongest, and the other peaks are almost disappeared. These results mean that the current density alters the texture of the composites and enhances the (200) reflections, which is in good agreement with the literature reported observation (the current efficiency of Ni deposition reached high values of over 97%) [26]. XRD analyses show that the texture coefficient of the deposits varies with current density. From Figure 7b and Table 3, the calculated results exhibit that the texture coefficient of (111) and (220) orientation decreases from 0.91 to 0.05 and 0.43 to 0.18, respectively; while the (200) orientation index increases from 0.66 to 2.9.

The variation of preferred orientation implied two possible reasons. One is the growth axis of the nickel grain mainly depends on the applied current density. There is a trend for dominating surface textures with increasing current density, as follows—(110) < (211) < (100). This means that

(110), (211) and (100) texture are preferred orientation at very low current, medium and high current, respectively [27]. This also can be explained by the theory of nucleation energy (W_{hkl}) [28,29] as Equation (2).

$$W_{hkl} = \frac{B_{hkl}}{\frac{zF}{Na} \eta - A_{hkl}}, \tag{2}$$

where A_{hkl} and B_{hkl} are material parameters of the crystallographic direction (hkl); Na and F are the constant of Avogadro and Faraday, respectively; z is the number of electrons, and η is the over-voltage of cathodic polarization. For face-centered cubic metals, at low over-voltage, $W_{111} < W_{100} < W_{110}$, while $W_{100} < W_{111}$ at high over-voltage [26]. This phenomenon indicates that when particular nucleation energy is lower than other types of nucleation energy, the crystals of the deposited metal will exhibit particular preferred orientation. The other is the incorporated whiskers provides the occurrence of new nuclei and limits the growth of the original crystal grains [30,31], which facilitates more nucleation sites and the grain size refined. As mentioned above, the crystalline structure of Ni-W/SiC deposits is also affected by the factor of the SiCw content in the composites.

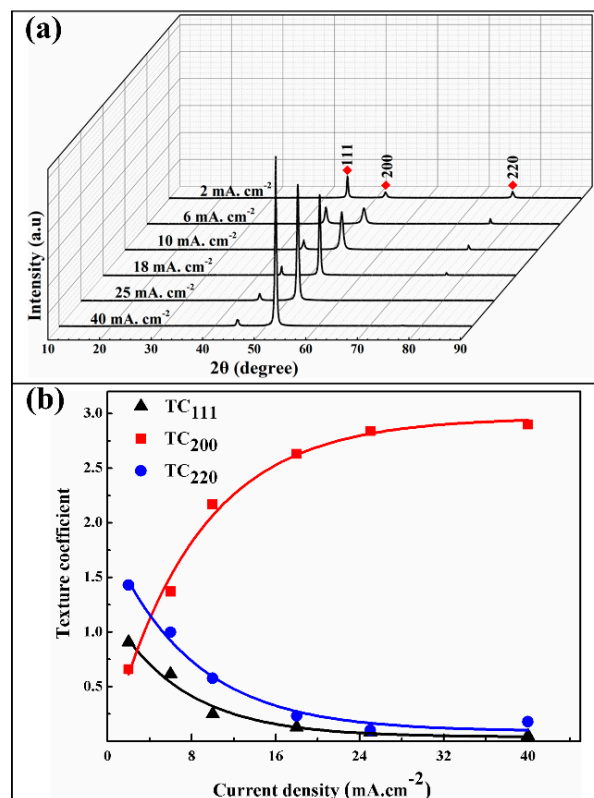


Figure 7. (a) XRD patterns of composites fabricated at a different current density, (b) The crystallographic orientation indexes of (111), (200) and (220).

Table 3. Texture coefficients of various (hkl) for the composite coatings as deposited at different current density.

(hkl)	$TC_{(hkl)}$					
	$2 \text{ mA}\cdot\text{cm}^{-2}$	$6 \text{ mA}\cdot\text{cm}^{-2}$	$10 \text{ mA}\cdot\text{cm}^{-2}$	$18 \text{ mA}\cdot\text{cm}^{-2}$	$25 \text{ mA}\cdot\text{cm}^{-2}$	$40 \text{ mA}\cdot\text{cm}^{-2}$
111	0.91	0.62	0.25	0.13	0.08	0.05
200	0.66	1.73	2.17	2.63	2.84	2.9
220	1.43	1	0.58	0.23	0.1	0.18

Figure 8 shows the XRD patterns and its crystallographic orientation indexes of the Ni/SiCw composite coatings electroplated at 20, 30, 40, 50, 60 °C, respectively. With the temperature elevated,

the intensity of the (200) increases, while (111), (220) peaks increases. The calculated orientation index of (200) plan increases from 1.08 to 2.32, while the (111) and (220) orientation index decreases from 1.15 to 0.32 and 0.73 to 0.36 (Figure 8b and Table 4), respectively. These results indicate that relative high electrolyte temperature is benefit for the preferred orientation of (200) plan, which is in agreement with previous studies [32].

In the view of the observations made by E. Budevski et al. [28], the energy barrier of nucleation showed a positive linear dependence with $1/\eta$ and $1/\eta^2$ for the 2D and 3D model, respectively; the nucleation kinetics of nickel crystallites depends on the applied overpotential η . At low overvoltage, the particles near the cathode suppress metal ion reduction; while at high overvoltage, the transmission of the metal ions to the cathode becomes an important factor, moreover, the incorporated of inert whiskers enhance this transmission [23]. Therefore, the grains size of composites at high temperature becomes larger than that at low temperature (Figure 2).

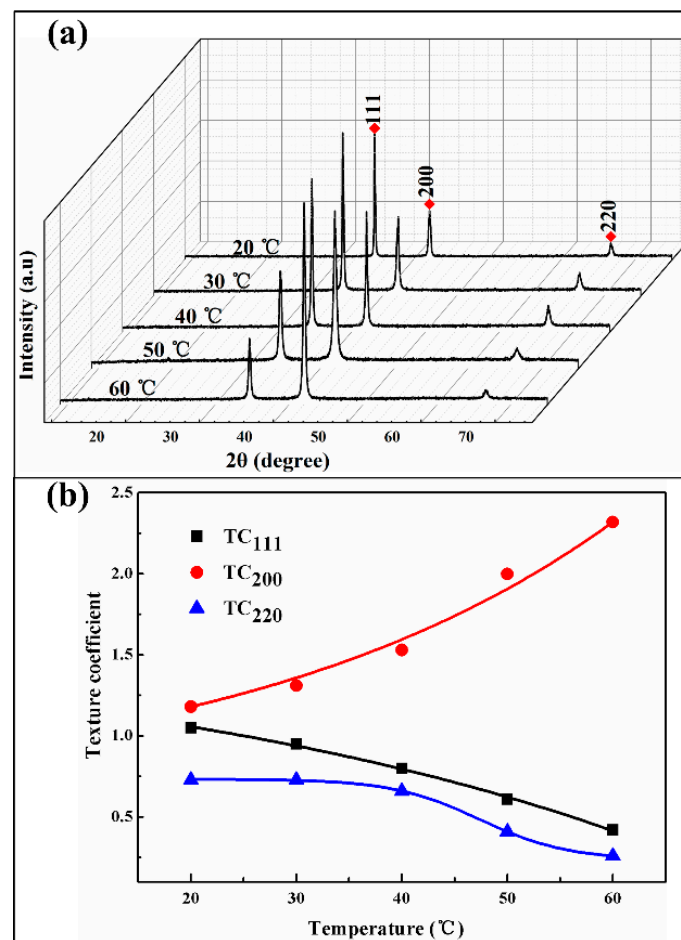


Figure 8. (a) XRD patterns of composites fabricated at a different temperature, (b) The crystallographic orientation indexes of (111), (200) and (220).

Table 4. Texture coefficients of various (hkl) for the composite coatings as deposited at different temperature.

(hkl)	TC _(hkl)				
	20 °C	30 °C	40 °C	50 °C	60 °C
111	1.15	1.05	0.8	0.51	0.32
200	1.08	1.21	1.53	2	2.32
220	0.73	0.73	0.71	0.51	0.36

Figure 9 shows the XRD patterns and its crystallographic orientation indexes of the Ni/SiC_w composite coatings electroplated under different stirring conditions. The XRD patterns (Figure 9a) shows that, under static conditions, the intensity of (200) peak is slightly higher than that of (220) peak, and (111) peak possess the highest intensity. When given a certain stirring speed at 100 rpm, there is about the same intensity of (111) and (200) crystal planes, while the intensity of (220) peak is very weak and almost disappeared. With increasing stirring speed to 300 rpm, the intensity of (200) peaks gradually increase, along with a relative decrease in intensity of (111) and (220) peaks. Notably, at high stirring speed (500 rpm), the intensity of (200) peak presents a weakening trend. This is because the excessive stirring speed takes a large impact force for the cathode surface, it can, therefore, caused the whiskers transferred with the electrolyte at a high speed. Ultimately, the content of whiskers incorporated into the nickel matrix is reduced. The XRD patterns further analysis is shown in Figure 9b and Table 5. The preferred orientation of the composite coating at different stirring speeds is mainly related to the content of SiC_w in coatings, and thereby the embedded SiC whiskers into the nickel matrix change the microstructure of the composites.

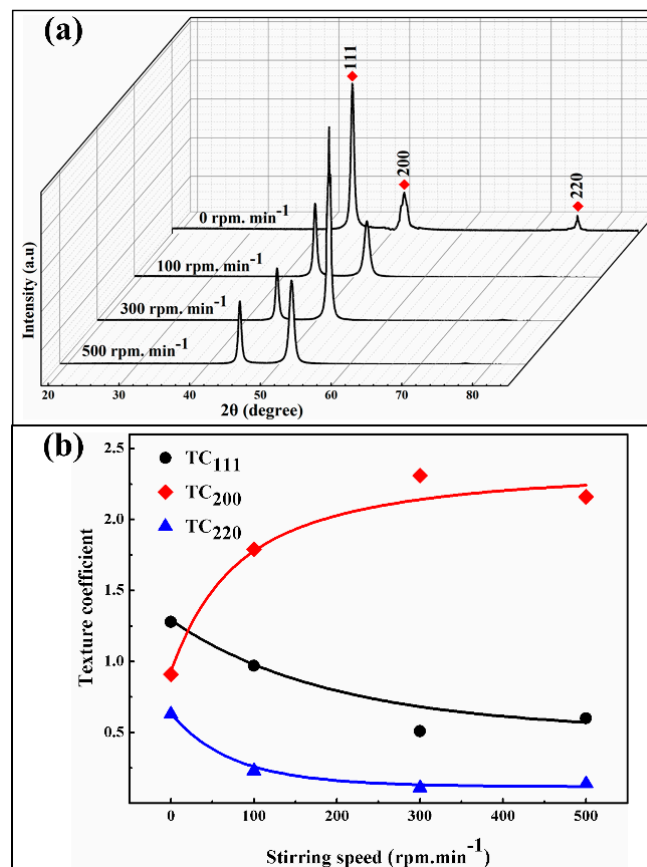


Figure 9. (a) XRD patterns of composites fabricated at a different stirring speed; (b) the crystallographic orientation indexes of (111), (200) and (220).

Table 5. Texture coefficients of various (hkl) for the composite coatings as deposited at different stirring speed.

(hkl)	TC _(hkl)			
	0 rpm	100 rpm	300 rpm	500 rpm
111	1.28	0.97	0.31	0.69
200	0.88	1.79	2.58	2.16
220	0.83	0.23	0.11	0.14

4. Conclusions

In summary, the influences of the external conditions of electrodeposition on the crystallographic texture, morphology and composition were investigated. For the deposited Ni/SiCw composite coatings, the content of SiCw in coatings increased with the increasing current density, stirring rate and electrolyte temperature in a certain range. Particularly, glossy Ni matrix surface with uniformly distributed whiskers was obtained at a current density of 18 mA/cm², whereas it became nodular and inhomogeneous with the widely differed spherical particles. Moreover, the detailed XRD analysis indicated that the current density altered the texture of the composites and enhanced the reflections of (200) plane. Also, the optimized temperature results revealed that the flat and bright morphology, as well as high content of whiskers in the composite coatings, was obtained at a temperature of 50 °C. Furthermore, the effects of stirring speed on the composition and structure on the coatings were studied. It was found that when the stirring speed was too low, the composite coatings appeared dendrites or nodules, while the whisker content was drastically reduced at a high speed. Consequently, these external conditions not only affect the surface morphology and the SiCw content of the composites, but also modified their preferred orientation.

Author Contributions: Conceptualization, G.D. and L.L.; methodology, L.L. and H.W.; software, L.L. and Y.S.; validation, G.D.; formal analysis, L.L. and H.W.; investigation, Z.Y. and Y.S.; resources, G.D.; data curation, L.L. and G.D.; writing—original draft preparation, L.L.; writing—review and editing, L.L. and G.D.; visualization, H.W.; supervision, Y.Z.; project administration, G.D.; funding acquisition, G.D.

Funding: This research was funded and supported by the National Natural Science Foundation of China (No. 61571287).

Acknowledgments: The authors would like to thank supports from the Shanghai Professional Technical Service Platform for Non-Silicon Micro-Nano Integrated Manufacturing.

Conflicts of Interest: The authors declare no conflict of interest.

References

1. Li, B.; Zhang, W.; Zhang, W.; Huan, Y. Preparation of Ni-W/SiC nanocomposite coatings by electrochemical deposition. *J. Alloy. Compd.* **2017**, *702*, 38–50. [[CrossRef](#)]
2. Fink, C.G.; Gray, O.H. Co-Deposition of Lead and Bismuth. *Trans. Electrochem. Soc.* **1932**, *62*, 123. [[CrossRef](#)]
3. Grazen, A.E. Method for Electroforming and Coating. U.S. Patent No. 3,061,525, 30 October 1962.
4. Ekmekci, D.; Bülbül, F. Preparation and characterization of electroless Ni-B/nano-SiO₂, Al₂O₃, TiO₂ and CuO composite coatings. *Bull. Mater. Sci.* **2015**, *38*, 761–768. [[CrossRef](#)]
5. Madah, F.; Dehghanian, C.; Amadeh, A.A. Investigations on the wear mechanisms of electroless Ni-B coating during dry sliding and endurance life of the worn surfaces. *Surf. Coat. Technol.* **2015**, *282*, 6–15. [[CrossRef](#)]
6. Zhang, W.; Li, B. Influence of electrodeposition conditions on the microstructure and hardness of Ni-B/SiC nanocomposite coatings. *Int. J. Electrochem. Sci.* **2018**, *13*, 3486–3500. [[CrossRef](#)]
7. Moghadam, A.D.; Omrani, E.; Menezes, P.L.; Rohatgi, P.K. Mechanical and tribological properties of self-lubricating metal matrix nanocomposites reinforced by carbon nanotubes (CNTs) and graphene—A review. *Compos. Part B* **2015**, *77*, 402–420. [[CrossRef](#)]
8. Snead, L.L.; Nozawa, T.; Katoh, Y.; Byun, T.S.; Kondo, S.; Petti, D.A. Handbook of SiC properties for fuel performance modeling. *J. Nucl. Mater.* **2007**, *371*, 329–377. [[CrossRef](#)]
9. Benea, L.; Bonora, P.L.; Borello, A.; Martelli, S. Wear corrosion properties of nano-structured SiC–nickel composite coatings obtained by electroplating. *Wear* **2001**, *249*, 995–1003. [[CrossRef](#)]
10. Benea, L.; Wenger, F.; Ponthiaux, P.; Celis, J.P. Tribocorrosion behaviour of Ni–SiC nano-structured composite coatings obtained by electrodeposition. *Wear* **2009**, *266*, 398–405. [[CrossRef](#)]
11. Lekka, M.; Kouloumbi, N.; Gajo, M.; Bonora, P.L. Corrosion and wear resistant electrodeposited composite coatings. *Electrochim. Acta* **2005**, *50*, 4551–4556. [[CrossRef](#)]
12. Ye, Z.; He, Q.; Lang, Y.; Chen, Y.; Liu, L.; Chen, C.; Ma, G. The effect of current density on the corrosion resistance and wear resistance of electrodeposition silver–Graphite composite coating. *J. Funct. Mater.* **2016**, *47*, 08227–08231.

13. Hai, J.C.; Tam, J.; Kovylyna, M.; Kim, Y.J.; Erb, U. Thermal conductivity of bulk nanocrystalline nickel-diamond composites produced by electrodeposition. *J. Alloy. Compd.* **2016**, *687*, 570–578.
14. Jun, C.H.; Young, J.K.; Uwe, E. Thermal conductivity of copper-Diamond composite materials produced by electrodeposition and the effect of TiC coatings on diamond particles. *Compos. Part B* **2018**, *155*, 197–203.
15. Ueda, M.; Arai, S. Fabrication of High Thermal Conductivity Cu/Diamond Composites by Electrodeposition. *Electrochem. Soc.* **2014**, *49*, 2220.
16. Gül, H.; Kılıç, F.; Uysal, M.; Aslan, S.; Alp, A.; Akbulut, H. Effect of particle concentration on the structure and tribological properties of submicron particle SiC reinforced Ni metal matrix composite (MMC) coatings produced by electrodeposition. *Appl. Surf. Sci.* **2012**, *258*, 4260–4267. [[CrossRef](#)]
17. Gyftou, P.; Pavlatou, E.; Spyrellis, N. Effect of pulse electrodeposition parameters on the properties of Ni/nano-SiC composites. *Appl. Surf. Sci.* **2008**, *254*, 5910–5916. [[CrossRef](#)]
18. Chung, C.K.; Chang, W.; Chen, C.; Liao, M. Effect of temperature on the evolution of diffusivity, microstructure and hardness of nanocrystalline nickel films electrodeposited at low temperatures. *Mater. Lett.* **2011**, *65*, 416–419. [[CrossRef](#)]
19. Borkar, T.; Harimkar, S.P. Effect of electrodeposition conditions and reinforcement content on microstructure and tribological properties of nickel composite coatings. *Surf. Coat. Technol.* **2011**, *205*, 4124–4134. [[CrossRef](#)]
20. Chen, N.; Cheng, L.; Liu, Y.; Fang, Y.; Li, M.; Gao, Z.; Zhang, L. Microstructure and properties of SiC w /SiC composites prepared by gel-Casting combined with precursor infiltration and pyrolysis. *Ceram. Int.* **2018**, *44*, 969–979. [[CrossRef](#)]
21. Harimkar, S.P.; Dahotre, N.B. Crystallographic and morphological textures in laser surface modified alumina ceramic. *J. Appl. Phys.* **2006**, *100*, 189. [[CrossRef](#)]
22. Hashemzadeh, M.; Raeissi, K.; Ashrafizadeh, F.; Khorsand, S. Effect of ammonium chloride on microstructure, super-hydrophobicity and corrosion resistance of nickel coatings. *Surf. Coat. Technol.* **2015**, *283*, 318–328. [[CrossRef](#)]
23. Hovestad, A.; Janssen, L. Electrochemical codeposition of inert particles in a metallic matrix. *J. Appl. Electrochem.* **1995**, *25*, 519–527. [[CrossRef](#)]
24. Zhang, R.; Gao, L.; Guo, J. Preparation and characterization of coated nanoscale Cu/SiCp composite particles. *Ceram. Int.* **2004**, *30*, 401–404. [[CrossRef](#)]
25. Li, Y.; Wang, G.; Liu, S.; Zhao, S.; Zhang, K. The preparation of Ni/GO composite foils and the enhancement effects of GO in mechanical properties. *Compos. Part B* **2018**, *135*, 43–48. [[CrossRef](#)]
26. Burzyńska, L.; Rudnik, E.; Baz, L.; Kotula, M.; Sierpiński, Z.; Szymański, W. The influence of current density and bath composition on the electrodeposition of nickel and nickel/silicon carbide composite. *Trans. IMF* **2003**, *81*, 193–198. [[CrossRef](#)]
27. Amblard, J.; Epelboin, I.; Froment, M.; Maurin, G. Inhibition and nickel electrocrystallization. *J. Appl. Electrochem.* **1979**, *9*, 233–242. [[CrossRef](#)]
28. Budevski, E.; Staikov, G.; Lorenz, W. Electrocrystallization: Nucleation and growth phenomena. *Electrochim. Acta* **2000**, *45*, 2559–2574. [[CrossRef](#)]
29. Pangarov, N.; Velinov, V. The orientation of silver nuclei on a platinum substrate. *Electrochim. Acta* **1966**, *11*, 1753–1758. [[CrossRef](#)]
30. Momeni, M.; Hashemzadeh, S.; Mirhosseini, M.; Kazempour, A.; Hosseinizadeh, S. Preparation, characterisation, hardness and antibacterial properties of Zn–Ni–TiO₂ nanocomposites coatings. *Surf. Eng.* **2016**, *32*, 490–494. [[CrossRef](#)]
31. Niksefat, V.; Ghorbani, M. Mechanical and electrochemical properties of ultrasonic-assisted electroless deposition of Ni–B–TiO₂ composite coatings. *J. Alloy. Compd.* **2015**, *633*, 127–136. [[CrossRef](#)]
32. Wasekar, N.P.; Haridoss, P.; Seshadri, S.K.; Sundararajan, G. Influence of mode of electrodeposition, current density and saccharin on the microstructure and hardness of electrodeposited nanocrystalline nickel coatings. *Surf. Coat. Technol.* **2016**, *291*, 130–140. [[CrossRef](#)]

